Secondary D-^{3}He Proton Spectra from D_2-Filled OMEGA Targets

Introduction

Two new diagnostic techniques now provide the first high-quality spectra of secondary fusion protons from imploded D_2-filled capsules in inertial confinement fusion (ICF) experiments. The potential utility of secondary neutrons and protons for diagnosing such capsules has been recognized for more than two decades,[1–8] but practical use of protons has previously been limited by the lack of accurate spectroscopic measurements. The first new technique utilizes a magnet-based charged-particle spectrometer; the second involves "wedge-range-filter"–based spectrometers utilizing special filters and CR39 nuclear track detectors. These spectrometers were recently used to acquire data from target capsules with about 14 atm of D_2 fuel in 19-μm-CH shells, imploded at the 60-beam OMEGA laser facility by irradiation with 22 kJ of laser energy. Results of that work, presented in this article, are important for the information they give about current experiments and for the potential they show for characterization of the cryogenic D_2-filled capsules to be used in the near future.

The general value of charged-particle spectrometry for capsule diagnostics has recently been demonstrated with magnet-based charged-particle spectrometers (CPS's), which are now used on a regular basis to measure spectra of primary fusion products (p, D, T, α) and "knock-on" particles (p, D, T, and ^{3}He elastically scattered by 14.1-MeV neutrons[3])[9,10] for a wide range of capsule types and implosion conditions on OMEGA.[11] Measured spectra provide a number of important implosion parameters such as primary yields, fuel ion temperature, and areal density (ρR) of fuel, shell(s), or fuel plus shell. Areal densities are determined by measuring the energy loss of charged fusion products as they pass out through the fuel and shell[9] or by measuring the yields of knock-on particles.[10]

In the most important future ICF experiments utilizing cryogenic capsules with DT or D_2 fuel, large areal densities will limit the number of diagnostic measurements that can be made of charged particles. On the National Ignition Facility (NIF), ρR_{total} of imploded DT capsules is eventually expected to exceed 1 g/cm^2. In this case, the only charged particles that could escape and be detected for studying ρR are tertiary protons,[12] which have energies as high as 30.8 MeV. DT capsules planned for OMEGA may (based on 1-D simulations) reach ρR_{total} of 0.2 to 0.3 g/cm^2. In this case, knock-on deuterons and tritons, resulting from elastic collisions with primary 14.1-MeV neutrons, could be detected and used to study ρR with CPS's.[10]

In the shorter term, cryogenic experiments will be carried out with pure-D_2 fuel. No charged primary fusion products will be energetic enough to escape and be detected, and there will be no high-energy primary neutrons to generate energetic knock-on particles. In addition, the method of determining ρR_{fuel} by measuring secondary-neutron yields[6] will fail for $\rho R_{\text{fuel}} \gtrsim 0.1$ g/cm^2. Fortunately, secondary D-^{3}He protons (12.6 to 17.5 MeV) *will* escape from D_2-filled capsules with relatively high ρR. These protons are created in the two steps indicated in reactions (1) and (2):

$$\mathrm{D} + \mathrm{D} \rightarrow n\,(2.45\ \mathrm{MeV}) + {}^3\mathrm{He}\,(0.82\ \mathrm{MeV}); \tag{1}$$

$${}^3\mathrm{He}\,(0.82\ \mathrm{MeV}) + \mathrm{D} \rightarrow \alpha\,(6.6\ \text{to}\ 1.7\ \mathrm{MeV}) + p\,(12.6\ \text{to}\ 17.5\ \mathrm{MeV}). \tag{2}$$

In one of the primary branches of the D-D reaction, ^{3}He is created with 0.82 MeV of kinetic energy. Some of the ^{3}He ions then react in-flight with thermal D ions, creating protons that, because of the kinetic energy of the ^{3}He, have a range of energies. Measured spectra of these protons can be used to measure ρR_{fuel} and ρR_{total}.

The remainder of this article will discuss the use of spectral measurements. Although the emphasis throughout is on secondary protons, there is also discussion of how they relate to the secondary neutrons created through reactions (3) and (4):

$$\mathrm{D} + \mathrm{D} \rightarrow p\,(3.02\ \mathrm{MeV}) + \mathrm{T}\,(1.01\ \mathrm{MeV}); \tag{3}$$

$$\mathrm{T}(1.01\ \mathrm{MeV}) + \mathrm{D} \rightarrow \alpha(6.7\ \text{to}\ 1.4\ \mathrm{MeV}) + n(11.9\ \text{to}\ 17.2\ \mathrm{MeV}). \quad (4)$$

The following sections discuss (1) how the characteristics of secondaries are related to the physical parameters of capsules; (2) how accurately measured spectra of secondary protons are made with the magnet-based CPS's and with "wedge-range-filter"–based spectrometers; (3) measurements during OMEGA shots; (4) physical interpretation of data; and (5) future application to cryogenic-target experiments.

Secondary Spectra and Capsule Characteristics

Two simple models of plasma structure are used here to illustrate how measurements of secondary yields and spectra are related to properties of compressed capsules. In the "hot-spot" model, all primary fusion reactions take place in a small region at the center of the spherical fuel, and the fuel outside the hot spot, where the primary fusion products react with cooler fuel to create secondaries, has uniform density and temperature. In the "uniform" model, the fuel is uniform over its entire spherical volume so that primary and secondary reactions take place everywhere. In both cases, there can be a spherical shell or pusher of a different material outside the fuel (generally CH, in most current OMEGA experiments). It is assumed in these simple models that the capsule is spherically symmetric, with no mixing of fuel and shell material, although numerical work currently underway indicates that fuel/shell mixing could be important. In future work, more-sophisticated models will be used.

The slowing down of primary ^{3}He and T in D fuel is modeled with the formalism described in Ref. 13, with results shown in Fig. 83.14. The production rates for secondaries are then determined by the cross sections shown in Fig. 83.15 (calculated from Ref. 14). The resultant yields, and the shapes of spectra as they are created in the fuel, are discussed below. Modifications to the spectrum of protons as they slow down on their way out of the fuel and shell are then determined by the stopping power illustrated in Fig. 83.16 (calculated according to Ref. 13).

1. Yields

By integrating over the appropriate paths of primary fusion products ^{3}He and T and using the foregoing assumptions to calculate their energies as a function of position, and then utilizing the secondary production rates, we can calculate yields Y_{2p} and Y_{2n} of secondary protons and neutrons as fractions of the primary-neutron yield Y_{1n} and obtain the results shown in Fig. 83.17. Related calculations were carried out previously[1–8] for some of these cases, utilizing older models for the slowing down of ^{3}He and T. The authors pointed out that a nearly linear relationship exists between ρR_{fuel} and the secondary-to-primary-yield ratios as long as ρR_{fuel} is low enough that the primary particles (^{3}He or T) escape the fuel. Each yield ratio reaches a saturation level (as shown in Fig. 83.17) when the appropriate primary particle is completely slowed down in the fuel, but measurements of yield can be used to infer ρR_{fuel} as long as saturation has not been reached. The results are weakly dependent on plasma density, but the plasma temperature has a strong impact on the value of ρR_{fuel} at which the linear relationship fails because of com-

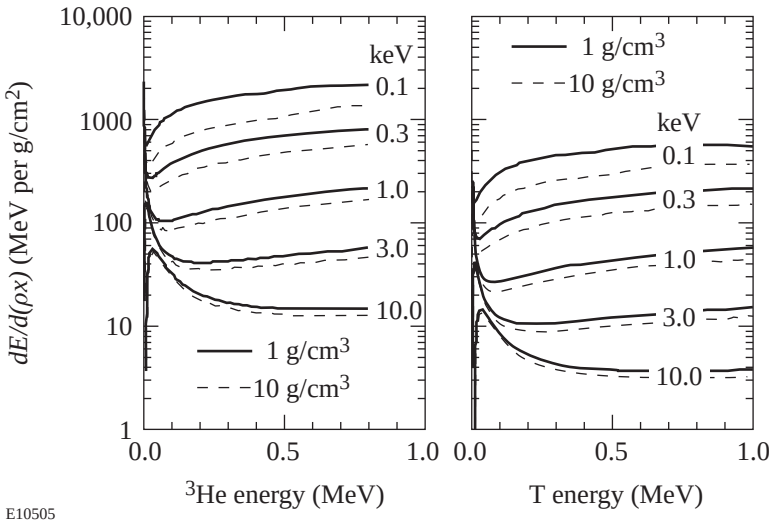

Figure 83.14
Stopping powers for ^{3}He (left) and T (right) in D plasmas of various temperatures (calculated according to Ref. 13). Note that at higher temperatures there is an important peak in the stopping power at low energies, due to ion-induced slowing.

plete slowing down of the primary particles in the fuel. This is a consequence of the temperature dependence of the total particle ranges, as illustrated in Fig. 83.18. Because of the magnitude of the cross sections (Fig. 83.14), secondary protons are preferentially produced close to the birth position of primary ^{3}He, while secondary neutrons are preferentially created near the end of the range of the primary T (see Fig. 83.19).

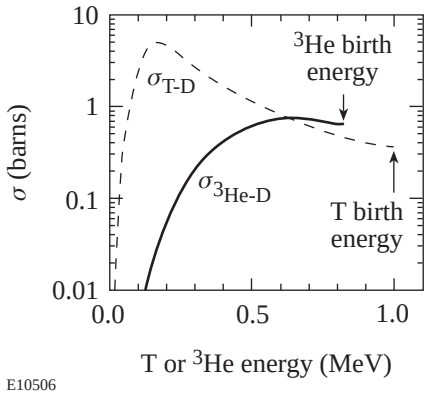

Figure 83.15
Fusion cross sections (σ) for energetic ^{3}He or T with cold D plasma (calculated according to information in Ref. 14).

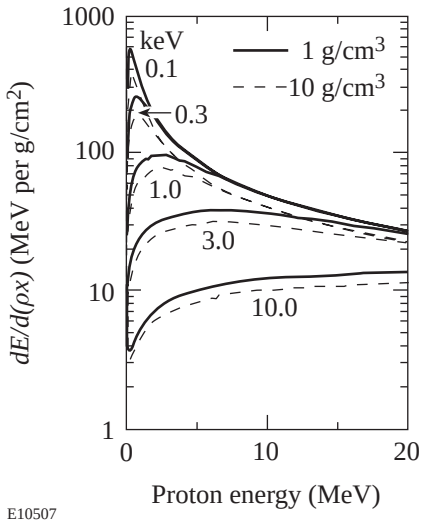

Figure 83.16
Stopping power for protons in D plasmas of various temperatures (calculated according to Ref. 13). The values for CH plasmas are almost identical except for being higher by a factor of about 14/13 (the ratio of the numbers of electrons per unit mass).

Two differences between the hot-spot and uniform models are apparent in Fig. 83.17: (1) The value of ρR_{fuel} for a given yield is slightly higher in the uniform model, reflecting the fact that the mean distance traveled by primary particles before they encounter the fuel–pusher interface is smaller by a factor of 0.75. (2) Complete saturation of yield at high values of ρR_{fuel} in the uniform model is approached asymptotically, but never reached, because some primaries are always created close enough to the surface to escape the fuel.

Although a measured secondary-proton yield can be used in the context of our models to infer ρR_{fuel} only in regimes where the primary ^{3}He escapes the fuel before stopping, another kind of information can be inferred when complete stopping occurs in the fuel. As seen in Fig. 83.17, the electron temperature T_e determines the maximum possible secondary-to-primary ratio Y_{2p}/Y_{1n}. If it is known that yield saturation has been reached, it is possible to estimate the effective electron temperature as illustrated in Fig. 83.20. A similar relationship between electron temperature and yield saturation holds for secondary neutrons.

2. Birth Spectra

Going beyond the calculation of yields, we can investigate the shapes of secondary-particle spectra at their birth. Consider first the protons. If ρR_{fuel} is small, so that primary ^{3}He particles escape the fuel before losing much of their 0.82-MeV birth energy, then the protons they produce by fusing with fuel deuterons are equally distributed between limiting energies of about 12.6 and 17.5 MeV. The energy limits are defined by kinematics and are determined by ^{3}He energy at the time of interaction with D. The flat distribution as a function of energy between the limits can be demonstrated by assuming that fusion products are distributed isotropically in the D–^{3}He center-of-mass frame, transforming to the lab frame, and calculating the number of particles per unit energy. The number of protons produced during the slowing down of ^{3}He from energy $E_{^3\text{He}}$ to $E_{^3\text{He}} - \Delta E_{^3\text{He}}$ is proportional to

$$\Delta E_{^3\text{He}} \sigma_{^3\text{He–D}}\left(E_{^3\text{He}}\right) \Big/ \left[dE_{^3\text{He}} / d(\rho x)\right],$$

where $\sigma_{^3\text{He–D}}\left(E_{^3\text{He}}\right)$ is as shown in Fig. 83.15, X is the distance along the trajectory of ^{3}He in the plasma, and $dE_{^3\text{He}} / d(\rho x)$ is as shown in Fig. 83.14.

For larger values of ρR_{fuel}, some of the ^{3}He will slow down before leaving the fuel; when they interact with the fuel, the kinematically defined width of the resultant proton spectrum

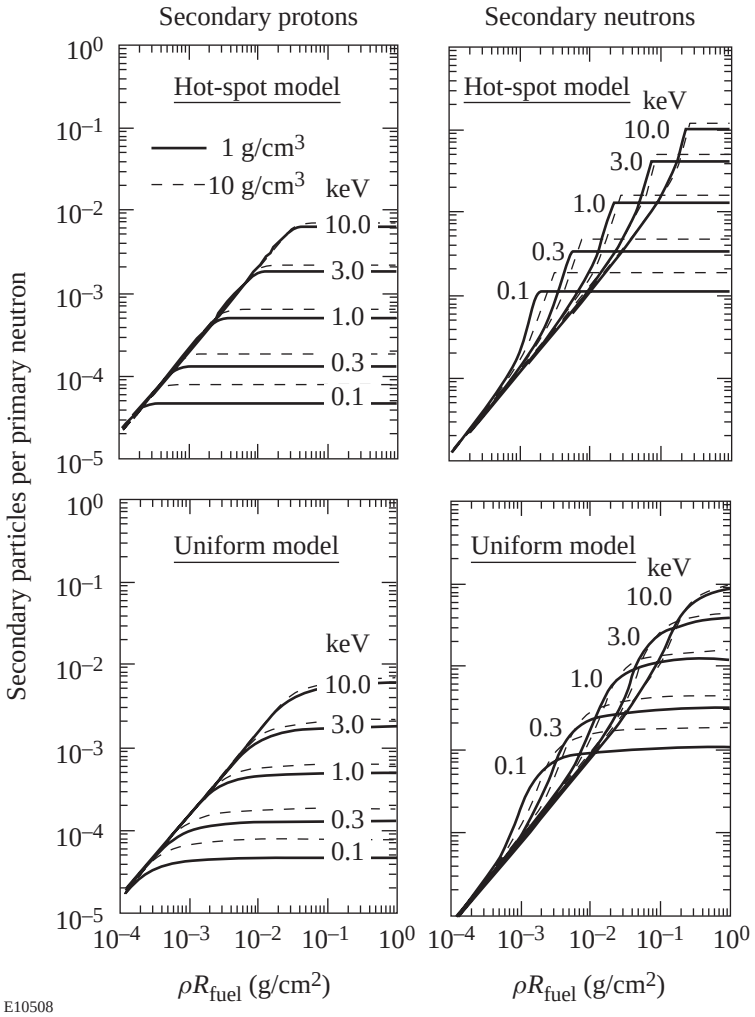

Figure 83.17
Yields of secondary protons (left) and neutrons (right), calculated using Li and Petrasso's ion-slowing formalism[13] to model the slowing down of primary fusion products in a D plasma. The two top plots assume the "hot-spot" model, in which all primary reactions take place in a small region at the center and secondary reactions take place outside the hot spot in a cooler region that is uniform in density and temperature. The two bottom plots assume the "uniform" model in which primary and secondary reactions take place throughout the uniform plasma. Plasma densities and electron temperatures T_e are as indicated.

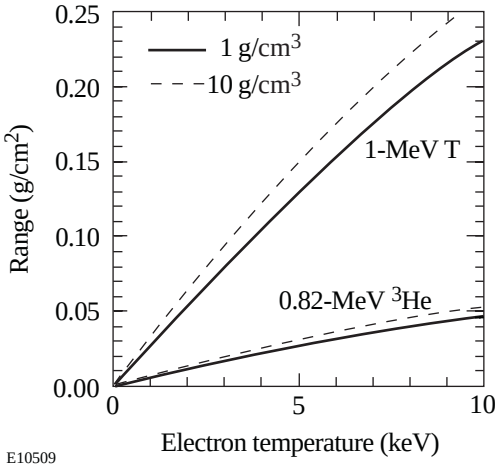

Figure 83.18
Ranges of primary D-D fusion products in a D plasma for different plasma densities and temperatures (from the stopping-power curves in Fig. 83.14).

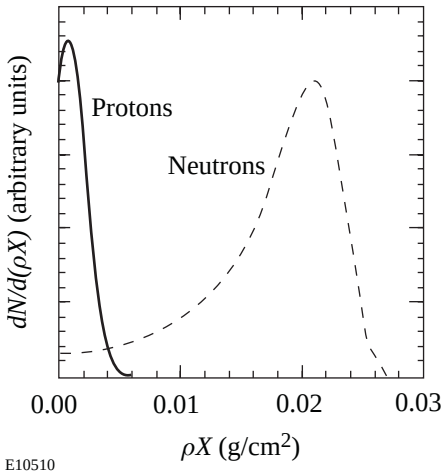

Figure 83.19
Illustration of how secondary protons are created mostly near the birth position of the primary ^{3}He, while secondary neutrons are created mostly toward the end of the range of primary T. The vertical axis is in arbitrary units that are different for the two curves; the horizontal axis unit ρX is the distance from primary birth position in g/cm^2 for a 1-keV, 3-g/cm^3 D plasma.

will be smaller. But since $\sigma_{^3\mathrm{He-D}}\left(E_{^3\mathrm{He}}\right)$ decreases rapidly as $E_{^3\mathrm{He}}$ goes below about 0.5 MeV, the contributions to the final proton spectrum become very small for lower-energy ^{3}He and the shape of the total proton spectrum remains relatively insensitive to the amount of slowing down, or equivalently the value of ρR_{fuel}. This is demonstrated in Fig. 83.21, which shows how, in the case of a hot-spot model, the shape of the spectrum gets built up as a contribution of parts due to ^{3}He slowed down by different amounts. Figure 83.21 also illustrates that the shape of the birth spectrum is relatively insensitive to the plasma temperature. The mean energy of the spectrum varies slightly with the amount of slowing down of ^{3}He, as shown in Fig. 83.22.

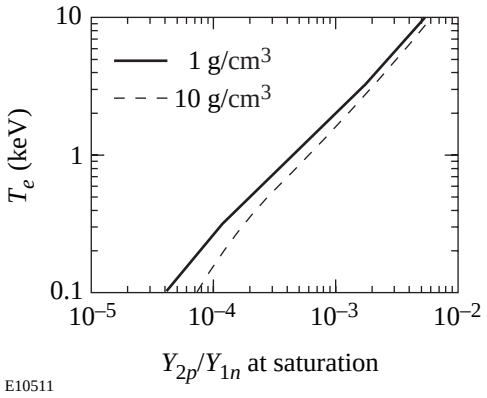

Figure 83.20
Electron temperature for which Y_{2p}/Y_{1n} cannot exceed a given saturation value (see Fig. 83.17). Under some circumstances, this relationship can be used to estimate T_e.

The secondary-neutron birth-spectrum shape is significantly more sensitive to ρR_{fuel} because the reaction cross section of primary T with fuel D increases rapidly as T energy decreases (down to about E_T = 0.2 MeV, as shown in Fig. 83.15). As discussed in Refs. 6–8, this means that the neutron spectrum gets narrower as ρR_{fuel} increases (and the exiting T energy decreases). Figure 83.21 illustrates this for the case of the hot-spot model.

3. Measured Spectra

A proton birth spectrum is never measured directly because it is modified by passage through the fuel and shell before being measured in a real experiment. Since the birth spectrum is relatively insensitive to fuel conditions, a measured spectrum contains diagnostic information about fuel and shell by virtue of the changes in the spectrum that can be inferred.

The mean energy of the secondary protons decreases according to the amount of material they traverse (Fig. 83.16

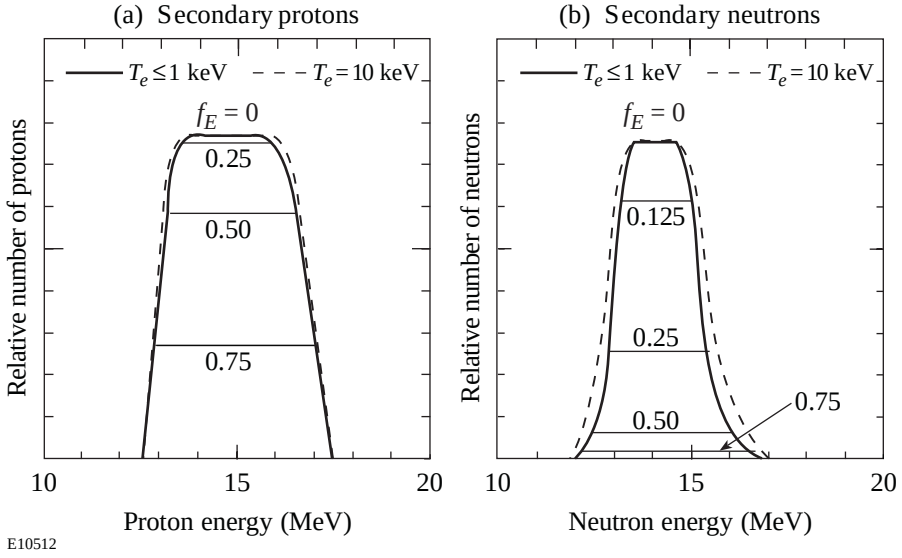

Figure 83.21
Calculated shapes of secondary-proton and -neutron spectra. These curves were generated by assuming that (a) the slowing of T or ^{3}He in a D plasma varies with energy as shown in Fig. 83.14, and (b) the primary particles are created near the center and pass through a uniform fuel that ranges their energies down to some fraction f_E of their birth energy (hot-spot model). The plasma density was assumed to be 3 g/cm^3. On each plot, the different curves show how the spectrum shape is built up as the primary particle gets ranged down; the curves *do not* show how the *number* of secondary particles varies with ρR. Each plot has one curve for plasma temperature 10 keV, corresponding to $f_E = 0$. This curve is arbitrarily normalized so its amplitude is the same as the corresponding curve for lower temperature to demonstrate that the shape is not strongly dependent on temperature.

showed how the stopping power of fuel or shell plasma for protons varies with proton energy and plasma temperature). For the case of a D plasma with ρ = 3 g/cm^3, Fig. 83.23 illustrates the slowing down of secondary protons as a function of T_e and ρX, where X is distance traveled through the plasma. The dependence on ρ is weak; the ratio of ρX to the mean energy loss $<\Delta E_{2p}>$ varies approximately as $\rho^{0.07}$ for $\rho X \leq 0.1$ g/cm^2. The dependence on temperature is weak for $T_e \leq 1$ keV and becomes progressively stronger for increasing T_e. For a CH plasma, the ratio of ρX to $<\Delta E_{2p}>$ is lower by about 13/14. If we assume that most of the protons are generated near the center of the fuel, then we can relate $<\Delta E_{2p}>$ to a sum of contributions from ρR_{fuel} and ρR_{shell}.

The protons are not all generated precisely at the center of the fuel, so they pass through slightly different amounts of material while leaving the capsule. This affects the mean energy, but that effect is fairly small for the OMEGA data discussed here. It also causes a broadening of the spectrum, and in future work that broadening will be used as another constraint on capsule structure.

A secondary-neutron birth spectrum can be measured directly.[15] The shape of this spectrum is sensitive to fuel conditions, so it has potential diagnostic value.[8] Figure 83.24 summarizes the plasma parameter regimes in which the measurement methods described above are applicable.

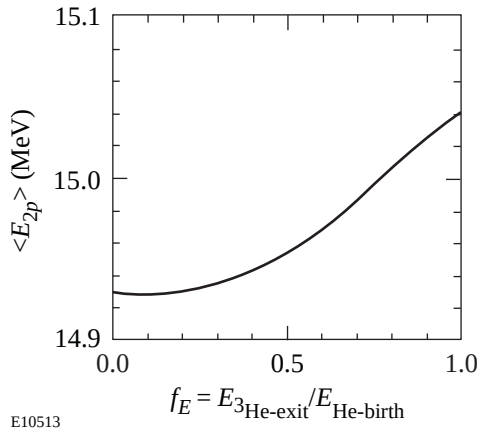

Figure 83.22
Dependence of the mean energies of the proton birth spectra (shown in Fig. 83.21) on the fraction of ^{3}He energy remaining when the ^{3}He reaches the fuel–pusher interface. Plasma temperature was assumed to be 3 keV, and the density was 3 g/cm^3. If the appropriate value of f_E (defined in the previous figure caption) is unknown, the effective mean energy will be uncertain. In such a case, we could use the value 14.97±0.04 MeV, which corresponds to the assumption of equal probability for all values of f_E.

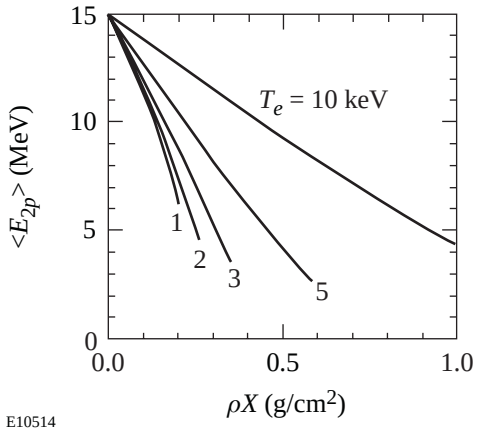

Figure 83.23
The mean energy of a secondary-proton spectrum after slowing down in a D plasma with ρ = 3 g/cm^3. The horizontal axis unit ρX is distance from birth position in g/cm^2. For a CH plasma, the value of ρX corresponding to a given energy should be reduced by the factor 13/14 (the ratio of electrons per unit mass for D to the value for CH). The dependence on ρ is weak; for $\rho X \leq 0.1$, the value of ρX corresponding to a given energy varies approximately as $\rho^{0.07}$.

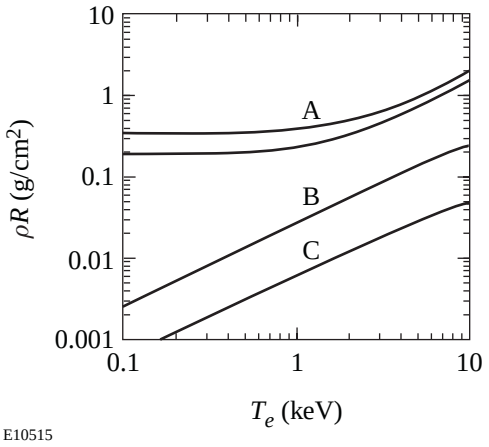

Figure 83.24
Boundaries of regimes in which various measurements can give diagnostic information about a 3-g/cm^3, pure-D plasma (assuming the hot-spot model). Note that ρR refers to ρR_{total} for curve A, but ρR_{fuel} for curves B and C. (A) Measurements of Y_{2p}/Y_{1n} and secondary-proton energy shift can be made only in the region *below* these curves, which show the ρR_{total} at which secondary protons fail to escape from the plasma (one curve each for the upper and lower limits of the birth spectrum). (B) Measurements of Y_{2n}/Y_{1n} give information about ρR_{fuel} only in the region *below* this curve, which shows where primary T is ranged out completely by the fuel and where the "saturated" regions of Fig. 83.17 are reached. *Above* this curve, measurement of Y_{2n} could give information about the fuel electron temperature. (C) Measurements of Y_{2p}/Y_{1n} give information about ρR_{fuel} only in the region *below* this curve, which shows where primary ^{3}He is ranged out completely by the fuel and where the saturated regions of Fig. 83.17 are reached. *Above* this curve, measurement of Y_{2p} can give information about the fuel electron temperature (see Fig. 83.20).

Instruments for Measuring Secondary-Proton Spectra

1. A Magnet-Based Charged-Particle Spectrometer

Two magnet-based spectrometers (CPS1 and CPS2) are installed on OMEGA. More information about CPS1 and CPS2 is available elsewhere,[16,17] but the principle of operation is illustrated in Fig. 83.25, which shows how a magnet is used to separate protons (or other charged particles) of different energies into different trajectories. The particles are stopped in CR39 nuclear track detectors, which are subsequently etched in a solution of NaOH and water, and then scanned with a microscope. A small hole appears at the location of the track of each individual proton. The position of a particle track gives the particle energy directly by virtue of the trajectory followed through the magnet. Final determination of an energy spectrum involves subtracting a background noise level, which includes neutron-induced noise and "intrinsic track noise." The neutron noise consists of tracks caused by protons elastically scattered by primary fusion neutrons, either in the CR39 itself or in surrounding materials; it scales with primary-neutron yield. The intrinsic track noise is caused by structural defects in the CR39, which look like particle tracks after etching; it is independent of implosion yields. Both types of noise are uniformly distributed on the CR39, subject to statistics.

Measuring secondary-proton spectra with CPS2 is more difficult than measuring other spectra, such as those of primary D-^{3}He protons,[9] for two reasons: (1) CR39 is not very sensitive to protons with energies higher than about 7 MeV, so when detecting protons with higher energies it is necessary to use a filter to range the protons down in energy just before they impact the detector. This is not difficult for primary D-^{3}He protons, which are nearly monoenergetic. But for the wide interval of incident energies associated with secondary protons, no single-filter thickness will range all protons down to the 0.5- to 7-MeV interval for which the detector is efficient. For this reason, a new filter whose thickness varies with position (or, equivalently, energy) was fabricated of aluminum. (2) Statistical noise is a significant problem. Typical primary D-D neutron yields in the OMEGA experiments have been of the order of 10^{11}, and the secondary-proton yield is usually in the vicinity of 10^8. With a spectrometer slit width of 3 mm, a slit length of 15 mm (perpendicular to the magnet dispersion direction), and a target-to-slit distance of 100 cm, the maximum total number of detected protons per shot is about 360—enough to give reasonable statistical errors for the total yield and the mean energy, but the error bars on individual energy bins in a spectrum will be large. In addition, the number of background noise events that must be subtracted is comparable to the number of true proton events, making the statistical noise even worse. After dispersion by the magnet, the 360 protons are spread out over an area of about 3 cm^2 on the CR39, giving 120 protons/cm^2. This has to be compared with noise that comes from intrinsic defects and from neutrons. Intrinsic noise events generally appear at a density of the order of 50 per cm^2. Neutron-induced events occur at about one per 10^4 neutrons, or about 45 per cm^2 on the CR39 (which is about 135 cm from the target); thus, for a single shot, the ratio of noise events to secondary-proton events is of the order of 1.

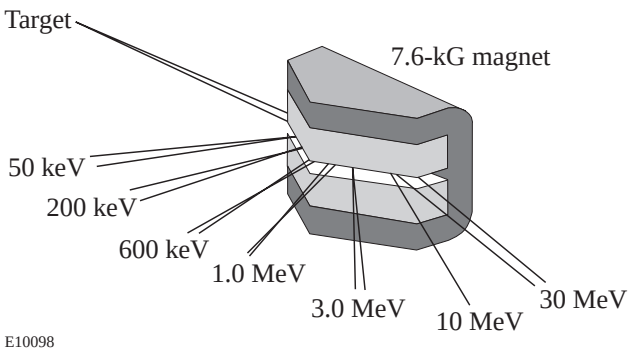

Figure 83.25
Concept of the magnet-based charged-particle spectrometers, showing how the magnetic field separates protons of different energies. Particles from the target capsule pass through a collimating aperture (not shown) before entering the magnet. After leaving the magnet, they are stopped in pieces of CR39 nuclear track detectors (not shown). The positions of the detected particles then indicate their energies by virtue of the trajectories followed.

2. Wedge-Range-Filter Spectrometers

Another new type of spectrometer, a wedge-range-filter spectrometer (WFS), has recently been tried for the first time. In a WFS (which will be described in detail elsewhere[18]), CR39 is again used as the particle detector, and special filters are used to range down the proton energies so they fall within the interval of sensitivity of the detector. The advantages of using range-filter measurements are simplicity and the ability to operate at lower yields by getting closer to the target. The disadvantages are (1) the interval of incident energies that can be detected with a single-filter thickness is not wide enough to cover the entire secondary-proton spectrum, and (2) it is difficult to get accurate spectral information. Secondary-proton yields have previously been estimated in this way by counting proton tracks behind a constant-thickness filter,[3–6] and Azechi *et al.*[6] used such data to make broadband estimates of different parts of the proton spectrum.

To find an improved approach, we have recently performed highly detailed calibrations of the response of CR39 to protons of different energies (different energies result in different track sizes)[19] and calibrations of the transmission characteristics of various filters. This information allows us to define a direct mapping between track diameter and incident proton energy for a given filter thickness. That mapping can be used to reconstruct part of the incident spectrum from a histogram of track diameters, but for each filter thickness the incident energy interval that is most accurately reconstructed is less than 1 MeV wide. To accurately reconstruct the entire secondary-proton spectrum, which is more than 5 MeV wide, it is necessary to have data from many different filter thicknesses. For this reason we use a special ranging filter with continuously varying thickness, making it possible to reconstruct a continuous spectrum over a wide energy interval. The filters used here were machined from aluminum, with thicknesses varying from 400 μm to 1800 μm. The fabrication tolerances turned out to be worse than desired, and the filters were slightly too thin. For the purposes of this first study, it was therefore necessary to estimate the thickness error by cross-calibrating the measured spectra with spectra acquired with the magnet-based CPS2. This single correction parameter was then applied to all data from WFS's. More-accurate fabrication and calibration techniques will make this unnecessary in the future.

A simple estimate of statistical errors can be made, assuming that a WFS is 15 cm from a capsule producing $Y_{1n} \simeq 10^{11}$ and $Y_{2p} \simeq 10^8$. With an effective area of about 3 cm^2 for the bulk of our spectrum, the number of incident protons will be about 10^5. These are spread out over at least 5 MeV, and at each filter thickness only about 1/3 of the spectrum is detected, so the number of protons actually counted is $\sim 3 \times 10^4$. This makes intrinsic noise totally irrelevant, but the number of neutron-induced events is $\sim 1 \times 10^4$. By restricting ourselves to an appropriate subset of track diameters, the number of proton events can be reduced by a factor of 2 and the number of neutron events by a factor of 4. The ratio of noise events to secondary-proton events is thus only ~0.15, and the large number of events guarantees very small statistical errors even after background subtraction.

Spectrum Measurements

1. Experiments

To illustrate the measurement and interpretation of secondary-proton spectra with our two new types of spectrometers, we present data from a recent series of four similar OMEGA shots. Table 83.I lists some basic shot parameters. The target capsules had ~14 atm of D_2 fuel in 19-μm-thick CH shells with outer diameters of ~910 μm. Each capsule was imploded by irradiation with ~22 kJ of 0.35-μm UV light applied in 60 beams for 1 ns (in a square-top pulse). The light was smoothed by spectral dispersion (2-D SSD with 0.3-THz bandwidth[20]). Primary-neutron yields Y_{1n} (measured via indium activation) varied from 8.1 to 9.8×10^{10}, while secondary-neutron yields Y_{2n} (measured with a time-of-flight diagnostic or Cu activation) were in the range of 1.1 to 1.8×10^8. Yield-weighted ion temperatures were 3.2 to 3.5 keV (measured with a neutron time-of-flight diagnostic).

CPS2 proton data were acquired by exposing one piece of CR39 to the protons from all four shots in order to sum the yields and minimize errors due to counting statistics. The background noise level was determined by measuring the number of apparent events at energies higher than the upper energy of the secondary-proton spectrum, and this mean noise level was subtracted from the total spectrum to give the results shown in Fig. 83.26. Table 83.I lists the mean energy and the yield of this proton spectrum.

WFS data for each of the four shots were taken at a distance of 15 cm from the target. Resultant spectra are shown in Fig. 83.27, and measured parameters are listed in Table 83.I. Figure 83.28 shows how the average of these spectra compares to the spectrum from the magnet-based CPS2.

2. Measurement Uncertainties

The proton yields obtained with CPS2 or with one of the WFS's have measurement uncertainties due to counting statistics. In addition, each measurement represents an average over a small solid angle, and measurements made at multiple positions during the same shot have shown that there are angular variations in particle fluxes that substantially exceed uncertainties due to counting statistics. This spatial variation

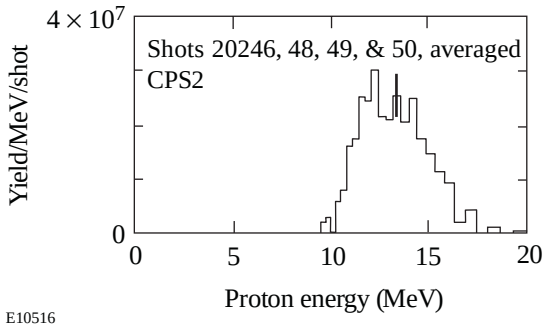

Figure 83.26
Spectrum of secondary protons for four shots, measured with the magnet-based spectrometer CPS2. One typical statistical error bar is shown.

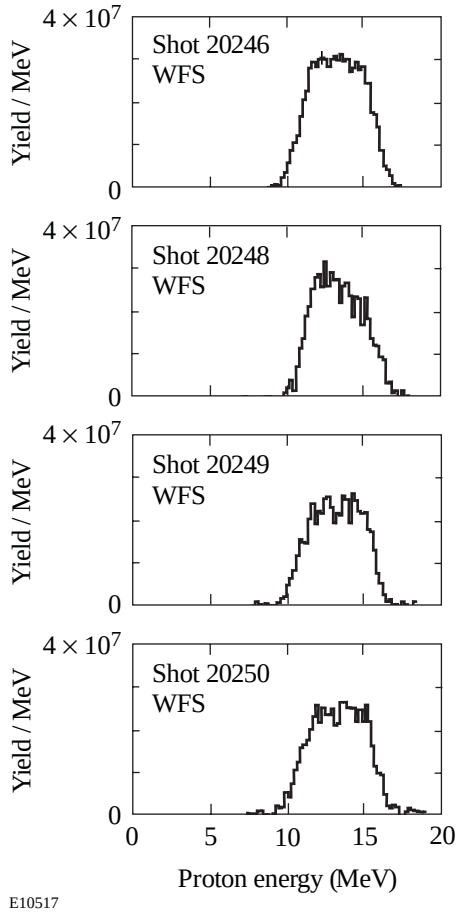

Figure 83.27
Spectra of secondary protons for the four individual OMEGA shots, as measured with the wedge-range-filter spectrometers (WFS's). One typical statistical error bar is shown in the top plot. The statistical errors in the lower three plots are slightly higher because only 1/3 of the available data were used.

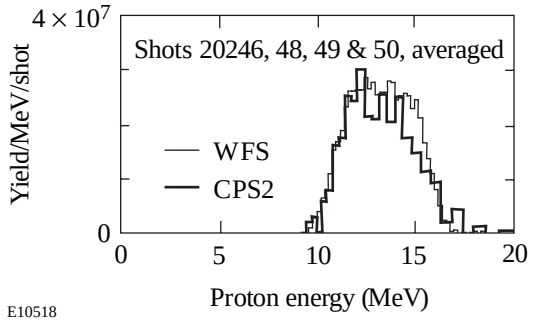

Figure 83.28
Comparison of the average spectrum measured with CPS2 (from Fig. 83.26) and the average of the individual WFS-measured spectra of Fig. 83.27.

of proton flux has been noted for a wide variety of shots and will be described in detail elsewhere. The standard deviation within measured spatial distributions of secondary-proton yield during individual shots tends to be in the vicinity of 20%. This puts a fundamental limit on the accuracy of any single yield measurement (as an indicator of total yield) and provides motivation for using multiple detectors.

The CPS2 yield measurements are affected by counting statistics in the measured spectra, including the subtracted background levels. The CPS2-measured proton-yield uncertainties quoted in Table 83.I were determined by adding, in quadrature, the statistical uncertainty (about 5%) and the expected standard deviation due to spatial variations (20% for a single shot, but 10% here for an average over four statistically independent shots). CPS2 measurements of mean energies have an uncertainty due to counting statistics (about 0.1 MeV here) and also due to any systematic energy calibration errors. Absolute calibration is accurate to about 0.1 MeV at 15 MeV.[21] The spatial variations in particle flux mentioned above do not seem to be accompanied by energy variations, so the energy measurement uncertainties quoted in Table 83.I are obtained by adding the statistical error to the calibration uncertainty in quadrature.

The WFS yield measurements are subject to the same 20% uncertainty due to spatial variations. Statistical errors for these measurements tend to be much smaller (near 1% for each shot), so in Table 83.I a 20% uncertainty is assigned to each individual measurement. Since there are four individual and statistically independent measurements (for the four shots), the error assigned to the shot-averaged yield is 10%. Errors in the measurement of mean energy are caused by counting statistics, but these statistical errors are quite small (about 0.02 MeV for shot 20246). The calibration error is larger, and since the energy calibration for these preliminary measurements was artificially tied to the calibration of the magnet-based CPS2, we do not list errors here (this will be remedied in the future).

3. Performance of the Spectrometer Types

Overall, the secondary-proton spectra obtained with the WFS's have less noise than those from CPS2. Statistical errors per shot are a factor of 10 smaller because the detector can be closer to the target, can use a larger active area, and has a higher ratio of true signal events to noise events. This advantage will diminish when secondary yields increase, as they are expected to for cryogenic targets. For current yields, the performance benefits combine with simplicity to make this approach very useful as a complement to the CPS's and particularly attractive

for studying the spectrum from many directions simultaneously for symmetry characteristics.[22] Theoretically, the WFS's should work at yields of ~10^6 and up to ~10^{10} (by moving farther from the target). They will not work for yields of 10^{11} or more, unless they can be moved well outside the target chamber, because of track overlap problems in the CR39. This probably limits their use to secondary (and tertiary) protons and, occasionally, primary protons from low-yield D-^{3}He shots. The primary charged products of many other targets will have yields that are too high, and the measurement of knock-on particles from DT targets,[10] which is of great interest to the ICF program, requires a separation of different particle types (D, T, and *p*), which cannot be performed with this approach.[19] These are appropriate applications for the magnet-based CPS's.

Interpretation of Measured Proton Spectra

1. Yield and Fuel Parameters

The measurements described above reflect properties of compressed targets, and in this section we look at implications

Table 83.I: OMEGA shot parameters, measurements, and inferred properties.

Parameter	Shot 20246	Shot 20248	Shot 20249	Shot 20250	<20246,48,49,50>
Fuel	14.2 atm D_2	14.3 atm D_2	14.3 atm D_2	14.3 atm D_2	14.3 atm D_2
Shell	19 μm CH	19 μm CH	19 μm CH	19 μm CH	19 μm CH
Outer Diameter	911 μm	909 μm	913 μm	905 μm	909.5 μm
Laser Energy	21.9 kJ	21.0 kJ	22.1 kJ	21.9 kJ	21.7 kJ
Laser Pulse	1 ns, square	1 ns, square	1 ns, square	1 ns, square	1 ns, square
T_i (keV)	3.2±0.5	3.5±0.5	3.5±0.5	3.2±0.5	3.3±0.5
Y_{1n} ($\times 10^{10}$)	9.76±0.07	8.06±0.06	8.28±0.06	9.17±0.07	8.82±0.03
Y_{2n} ($\times 10^{7}$)	17.7±1.2	11.6±0.9	11.1±0.9	12.4±1.0	13.1±0.5
Y_{2p} ($\times 10^{7}$)	15.8±3.1^{A,WFS}	11.8±2.4^{A,WFS}	12.1±2.4^{A,WFS}	12.1±2.4^{A,WFS}	11.4±1.3^{A,CPS2} 12.9±1.3^{A,WFS}
$\langle E_{2p}\rangle$ (MeV)	13.24^{B,WFS}	13.36^{B,WFS}	13.23^{B,WFS}	13.24^{B,WFS}	13.32±0.15^{CPS2} 13.27^{B,WFS}
ρR_{fuel} (mg/cm^2) from Y_{2n}/Y_{1n}	≤ (18±2)	≤ (15±2)	≤ (15±2)	≤ (14±2)	≤ (16±1)
ρR_{fuel} (mg/cm^2) from Y_{2p}/Y_{1n})	≥ (8±2)^{WFS}	≥ (7±2)^{WFS}	≥ (7±2)^{WFS}	≥ (6±2)^{WFS}	≥ (6±1)^{CPS2} ≥ (7±1)^{WPS}
ρR_{total} (mg/cm^2) from $\langle E_{2p}\rangle$	55$^{B,\ WFS}$	52$^{B,\ WFS}$	56$^{B,\ WFS}$	55$^{B,\ WFS}$	53±6^{CPS2} 54$^{B,\ WFS}$

^{CPS2}Measured with the magnet-based spectrometer CPS2.

^{WFS}Measured with a "wedge-range-filter" spectrometer.

^{A}Statistical errors are much smaller, but a 20% uncertainty is assumed because of known spatial nonuniformities (see pg. 138).

^{B}Statistical errors are very small, but systematic calibration errors have not been quantified (see pg. 138).

for physical parameters. The measured ratios Y_{2n}/Y_{1n} can be used to estimate ρR_{fuel}, with the information in Fig. 83.17, subject to two caveats. First, preliminary numerical simulations have suggested that any mixing at the shell–fuel boundary may result in an increase in secondary-neutron yield for a given ρR_{fuel}, meaning that the values in Fig. 83.17 could give us a value of ρR_{fuel} that is too high. For this reason, we will interpret our secondary-neutron-derived values of ρR_{fuel} as upper limits. Second, the results are slightly dependent on assumptions we make about temperature and density in the fuel. We know from neutron measurements that the ion temperatures are slightly higher than 3 keV; we assume the electron temperatures are the same. The mass density can't be determined directly, but we will find that the maximum possible value of ρR_{fuel} for these shots is about 18 mg/cm^2. This information can be used with the capsule dimensions and fill pressure to estimate that ρ is unlikely to exceed 10 g/cm^3. Inferred ρR_{fuel} increases slowly with increasing assumed ρ here, so using this upper limit on density will once again give us an upper limit on ρR_{fuel}. Since we don't know whether the radial profiles correspond more nearly to a uniform or hot-spot model, we can choose the larger results of the uniform model as an upper limit. Under these assumptions, we calculate upper limits on ρR_{fuel} in our four individual shots of 14 to 18 mg/cm^2, as listed in Table 83.I.

The measurements of Y_{2p}/Y_{1n} can also be used in conjunction with Fig. 83.17 to study ρR_{fuel}. In this case, there are reasons to interpret our results as lower limits. First, the values of Y_{2p}/Y_{1n} are very close to saturation. Second, preliminary work indicates that mixing at the shell–fuel boundary may sometimes result in a small decrease in secondary-proton yield for a given ρR_{fuel}, meaning that Fig. 83.17 could give us an inferred value of ρR_{fuel} that is too low. We therefore quote values from the hot-spot model (which gives lower numbers than the uniform model), using again the upper limit on ρ of 10 g/cm^3 (inferred ρR_{fuel} decreases slowly with increased assumed ρ here). The resulting lower limits for our shots fall in the interval from 6.3 to 8 mg/cm^2, as indicated in Table 83.I. These values are very similar to values for DT-filled capsules with similar shells and fill pressures, using CPS-measured spectra of knock-on particles.[10]

2. Energy Shift and ρR_{total}

The energy shift of a measured spectrum, relative to the birth spectrum, is due to proton slowing in both D fuel and CH shell. Figure 83.16 shows that the proton stopping powers normalized to ρ are almost the same for both D and CH, and in the vicinity of the birth energies of the protons there is little variation with plasma temperature for $T_e < 3$ keV. In addition, it will turn out that the shell ρR dominates the total ρR and that the amount of slowing down in the fuel is small. We therefore estimate ρR_{total} from the shift in mean energy by using the relationship for CH described in Fig. 83.23 and its caption, together with parameters appropriate for the shell. The result is weakly dependent on electron temperature and density in the shell, and we assume that $T_e = (1\pm0.5)$ keV and $\rho = (20\pm10)$ g/cm^3. These assumptions, together with the assumptions behind Fig. 83.23, lead to the inferred values of ρR_{total} shown in Table 83.I, which are all in the vicinity of 55 mg/cm^2. We note that this is similar to values measured for D-^{3}He–filled capsules and DT-filled capsules with similar shells and fill pressures.[9,10]

3. Future Improvements

Future data-interpretation work will involve more-detailed analytical and numerical modeling and the utilization of more information from proton spectra. The WFS-measured spectra for single shots are clean enough to allow detailed comparisons of spectrum shapes with model predictions. The important fact is that the combination of neutron and proton measurements provides a strong set of constraints that must be addressed in any complete model of the physics of capsule behavior.

Conclusions

We have shown the first detailed measurements of secondary-proton spectra from D_2-filled capsules in ICF experiments and demonstrated that charged-particle spectrometry can be used to provide useful diagnostic information about D_2-filled capsules in OMEGA. The energy downshift of a spectrum is directly related to the total areal density of the capsule, and the secondary-proton yield gives diagnostic information about fuel parameters such as the fuel areal density (especially in conjunction with primary- and secondary-neutron yields).

This first feasibility demonstration is particularly important because measurement of secondary-proton spectra may be the only diagnostic method for studying the areal densities of imploded, cryogenic D_2 capsules if ρR_{fuel} exceeds the limit for usefulness of secondary-neutron measurements (of the order of 0.1 g/cm^2, as shown in Figs. 83.17 and 83.24). It is expected that cryogenic, D_2-filled capsules will be imploded on OMEGA in the near future. Estimates of total areal densities, made from 1-D simulations, are as high as 0.2 to 0.3 g/cm^2. Under such circumstances, the measurement of secondary-proton spectra will still be possible with the techniques described here (and the increased yields will substantially decrease the statistical errors). This can be seen in Fig. 83.24, which

indicates the range of conditions under which the protons will escape the capsule and be measurable.

ACKNOWLEDGMENT

We thank Brock Bose for assistance in scanning CPS2 data. The work described in this article was performed in part at the LLE National Laser Users' Facility (NLUF) and was supported in part by U.S. Department of Energy Contract Number DE-FG03-99SF21782, LLE subcontract number PO410025G, LLNL subcontract number B313975, and the U.S. Department of Energy Office of Inertial Confinement Fusion under Cooperative Agreement No. DE-FC03-92SF19460. Part of this work was also performed under the auspices of the U.S. Department of Energy by University of California Lawrence Livermore National Laboratory under contract No. W-7405-Eng-48.

REFERENCES

1. H. D. Campbell and F. H. Southworth, in *1st Topical Meeting on the Technology of Controlled Nuclear Fusion* (American Nuclear Society, Hinsdale, IL, 1974), pp. 75–76.
2. E. G. Gamalii *et al.*, JETP Lett. **21**, 70 (1975).
3. S. Skupsky and S. Kacenjar, J. Appl. Phys. **52**, 2608 (1981).
4. T. E. Blue and D. B. Harris, Nucl. Sci. Eng. **77**, 463 (1981).
5. T. E. Blue *et al.*, J. Appl. Phys. **54**, 615 (1983).
6. H. Azechi *et al.*, Appl. Phys. Lett. **49**, 555 (1986).
7. H. Azechi, M. D. Cable, and R. O. Stapf, Laser Part. Beams **9**, 119 (1991).
8. M. D. Cable and S. P. Hatchett, J. Appl. Phys. **62**, 2233 (1987).
9. C. K. Li, D. G. Hicks, F. H. Séguin, J. A. Frenje, R. D. Petrasso, J. M. Soures, P. B. Radha, V. Yu. Glebov, C. Stoeckl, D. R. Harding, J. P. Knauer, R. L. Kremens, F. J. Marshall, D. D. Meyerhofer, S. Skupsky, S. Roberts, C. Sorce, T. C. Sangster, T. W. Philips, M. D. Cable, and R. J. Leeper, Phys. Plasmas **7**, 2578 (2000).
10. C. K. Li *et al.*, "Study of Direct-Drive, DT-Gas-Filled-Plastic-Capsule Implosions Using Nuclear Diagnostics on OMEGA," to be submitted to Physics of Plasmas.
11. T. R. Boehly, D. L. Brown, R. S. Craxton, R. L. Keck, J. P. Knauer, J. H. Kelly, T. J. Kessler, S. A. Kumpan, S. J. Loucks, S. A. Letzring, F. J. Marshall, R. L. McCrory, S. F. B. Morse, W. Seka, J. M. Soures, and C. P. Verdon, Opt. Commun. **133**, 495 (1997).
12. R. D. Petrasso, C. K. Li, M. D. Cable, S. M. Pollaine, S. W. Haan, T. P. Bernat, J. D. Kilkenny, S. Cremer, J. P. Knauer, C. P. Verdon, and R. L. Kremens, Phys. Rev. Lett. **77**, 2718 (1996).
13. C. K. Li and R. D. Petrasso, Phys. Rev. Lett. **70**, 3059 (1993).
14. S. Glasstone and R. H. Lovberg, *Controlled Thermonuclear Reactions: An Introduction to Theory and Experiment* (Van Nostrand, Princeton, NJ, 1960), Chap. 2.
15. F. J. Marshall, J. A. Delettrez, R. Epstein, V. Yu. Glebov, D. R. Harding, P. W. McKenty, D. D. Meyerhofer, P. B. Radha, W. Seka, S. Skupsky, V. A. Smalyuk, J. M. Soures, C. Stoeckl, R. P. Town, B. Yaakobi, C. K. Li, F. H. Séguin, D. G. Hicks, and R. D. Petrasso, Phys. Plasmas **7**, 2108 (2000).
16. D. G. Hicks, "Charged Particle Spectroscopy: A New Window on Inertial Confinement Fusion," Ph.D. thesis, Massachusetts Institute of Technology, 1999.
17. D. G. Hicks, C. K. Li, R. D. Petrasso, F. H. Séguin, B. E. Burke, J. P. Knauer, S. Cremer, R. L. Kremens, M. D. Cable, and T. W. Phillips, Rev. Sci. Instrum. **68**, 589 (1997).
18. F. H. Séguin *et al.*, "A Proton Spectrometer Based on a Wedge-Shaped Range Filter and CR-39 Nuclear Track Detectors," to be submitted to Review of Scientific Instruments.
19. J. A. Frenje *et al.*, "Charged Particle Measurements in DD, D^{3}He, and DT Implosions at the OMEGA Laser Facility Using Diagnostic Techniques Based on CR-39 Track Detection," to be submitted to Review of Scientific Instruments.
20. S. Skupsky and R. S. Craxton, Phys. Plasmas **6**, 2157 (1999).
21. D. G. Hicks *et al.*, "Charged-Particle Acceleration and Energy Loss in Laser-Produced Plasmas," to be published in Physics of Plasmas.
22. P. B. Radha, J. A. Delettrez, R. Epstein, S. Skupsky, J. M. Soures, S. Cremer, and R. D. Petrasso, Bull. Am. Phys. Soc. **44**, 194 (1999).